



Published in final edited form as:

Nature. 2011 April 21; 472(7343): 351–355. doi:10.1038/nature09865.

Neuronal activity is required for the development of specific cortical interneuron subtypes

Natalia V. De Marco García^{1,*}, Theofanis Karayannis^{1,*}, and Gord Fishell¹

¹Smilow Neuroscience Program, Departments of Cell Biology and Neural Science, New York University Langone Medical Center, New York, New York 10016, USA

Electrical activity has been shown to regulate development in a variety of species and in various structures¹, including the retina²⁻⁴, spinal cord⁵⁻⁶ and cortex⁵. Within the mammalian cortex specifically, the development of dendrites and commissural axons in pyramidal cells is activity-dependent⁷⁻⁸. However, little is known about the developmental role of activity in the other major cortical population of neurons, GABAergic interneurons. These neurons are morphologically and functionally heterogeneous and efforts over the past decade have focused on determining the mechanisms that contribute to this diversity⁹⁻¹¹. It was recently discovered that 30% of all cortical interneurons arise from a relatively novel source within the ventral telencephalon, the caudal ganglionic eminence (CGE)¹¹⁻¹². Due to their late birthdate, these interneurons populate the cortex only after the majority of other interneurons and pyramidal cells are already in place and have started to functionally integrate. Here we demonstrate that for CGE-derived Re⁺ and Cr⁺ (but not VIP⁺) interneurons¹²⁻¹³, activity is essential before postnatal day 3 (P3) for correct migration, and that after P3, glutamate-mediated activity controls the development of their axons and dendrites. Furthermore, we show that the engulfment and cell motility 1 gene (*Elmo1*)¹⁴, a target of the transcription factor distal-less homeobox 1 (*Dlx1*)¹⁵, is selectively expressed in Re⁺ and Cr⁺ interneurons and is both necessary and sufficient for activity-dependent interneuron migration. Our findings reveal a selective requirement for activity in shaping the cortical integration of specific neuronal subtypes.

Experimental evidence indicates that interneurons are electrically active shortly after their birth and participate in the early network activity that may contribute to circuit maturation in the neonatal cortex¹⁶⁻¹⁸. However, the role of activity in developing interneuron subtypes has not been addressed. Here we demonstrate that altering the level of neuronal excitability *in vivo* within genetically targeted CGE-derived interneurons has profound consequences on multiple aspects of the development of select subtypes within this population, as well as their associated gene expression (Supplementary Fig. 1).

Users may view, print, copy, download and text and data- mine the content in such documents, for the purposes of academic research, subject always to the full Conditions of use: http://www.nature.com/authors/editorial_policies/license.html#terms

Correspondence to: Dr. Gord Fishell¹ (fisheg01@nyumc.org).

*These authors contributed equally to this work

Author contribution. NVD and GF conceived the project. NVD and TK designed and carried out the experiments. NVD wrote the manuscript with the help of all authors.

Author information The authors declare no competing financial interests.

To suppress the neuronal excitability within CGE-derived interneurons, we electroporated *in utero* the inward rectifying potassium channel Kir2.1 under the control of the *Dlx5/6* enhancer element¹⁹ at e15.5, which results in selective expression within CGE-derived interneuron populations (Supplementary Fig. 2). Kir2.1-overexpression has been shown to affect activity by lowering the resting membrane potential (V_{rest}), therefore altering neuronal excitability²⁰. We detected expression of this channel by *in situ* hybridization (Supplementary Fig. 3a-b). To functionally assess the presence of membrane-targeted channels, we performed whole-cell patch clamp recordings from *Dlx5/6-Kir2.1*, *Dlx5/6-eGFP* co-electroporated interneurons in voltage clamp at P8-P9. I/V curve analysis indicated the presence of an inward rectifying potassium conductance that was active at V_{rest} and was blocked by 300 μ M barium, a concentration that preferentially blocks Kir2.1 channels (Supplementary Fig. 3d-g). Consistent with these observations, the V_{rest} of Kir2.1-electroporated interneurons was significantly more hyperpolarized than that of interneurons electroporated with eGFP alone (Supplementary Fig. 3c). By P8, subsets of the interneurons expressing the Kir2.1 channel showed pronounced defects in their morphologies (Fig. 1, Supplementary Fig. 4a-b and 5). To quantify alterations in dendrites and axons, we reconstructed interneuron morphologies from cortical slices at P8-P9, the earliest stages at which interneuron subtypes can be consistently delineated by expression of immunochemical markers. Our experiments revealed that the total length of axonal arbors was significantly reduced in multipolar and bipolar Cr^+ interneurons, as well as neurogliaform and dense plexus Re^+ subtypes, while those of multipolar VIP^+ interneurons remained unaltered (Fig. 1 and Supplementary Fig. 4a-b). Quantification of axonal nodes and ends (see Methods) also revealed scantily branched axons in Cr^+ and Re^+ subtypes but not in VIP^+ interneurons (Fig. 1b and Supplementary Fig. 5a-c). Although total dendritic length was not significantly decreased in Re^+ interneurons (Fig. 1c), this subtype exhibited less complex dendritic trees (Fig. 1c and Supplementary Fig. 5f). In contrast, VIP^+ and Cr^+ interneurons showed normal dendritic morphologies (Fig. 1c, and Supplementary Fig. 5d-e). To assess whether the morphological defects observed in Cr^+ and Re^+ interneurons were due to a developmental delay, we analyzed the electrophysiological properties and morphology of these interneurons at P15-19. Despite possessing mature intrinsic properties, Cr^+ and Re^+ interneurons at P15-19 displayed morphological defects similar to those found at P8 (Supplementary Fig. 4c-h). These findings suggest that the observed defects are unlikely to be a result of a developmental delay in maturation.

Although neuronal activity has been shown to be dispensable for the migration of pyramidal cells⁷, we noticed a pronounced overall shift in the laminar positioning of CGE subtypes expressing Kir2.1. CGE-derived interneurons migrate tangentially from the ventral telencephalon to the cortex where they then undergo radial migration to reach stereotypic positions in cortical laminae by P7. To assess the role of the neuronal activity during interneuron migration, we used a *tetO-Kir2.1.ires.LacZ* transgenic mouse line in which Kir2.1 and LacZ are expressed upon binding of the tet-transactivator (Tta) to the tetO element²⁰. We electroporated a *Dlx5/6-Tta* plasmid together with *Dlx5/6-eGFP*, again at e15.5 (Supplementary Fig. 6a), to induce Kir2.1 expression selectively in CGE-derived interneurons. These experiments revealed that the tangential migration of interneurons expressing Kir2.1 was indistinguishable from control populations at early developmental

stages (Fig. 2a). However, after P5, and in agreement with the constitutive *Dlx5/6-Kir2.1* electroporation experiment, interneurons that expressed Kir2.1 were found to occupy deeper cortical layers than control populations (Fig. 2a). To analyze the selectivity of this defect, we quantified the distribution of Cr⁺, Re⁺ and VIP⁺ interneurons across all cortical layers. We detected a significantly higher percentage of Kir2.1 Cr⁺ interneurons in layer IV and a concomitant reduction in the percentage of this population in layers II/III_t compared to controls (Fig. 2b). Similarly, in electroporated *tetO-Kir2.1.ires.LacZ* mice we observed a significantly lower percentage of Re⁺ interneurons in layer II/III_t and a subsequent increase in layer II/III_b compared to controls (Fig. 2b). In contrast, the distribution of VIP⁺ interneurons in electroporated *tetO-Kir2.1.ires.LacZ* mice was similar to that observed in controls (Fig. 2b). Our results indicate that neuronal activity is a determinant in the allocation of Cr⁺ and Re⁺ subtypes to defined cortical layers. One possible interpretation of our results is that the morphological defects observed in Cr⁺ and Re⁺ Kir2.1-expressing interneurons are an indirect consequence of the laminar mispositioning in the cortex. Alternatively, neuronal activity may regulate laminar migration and morphological maturation independently. To distinguish between these two possibilities, we took advantage of the ability of doxycycline (Dox) to suppress Kir2.1 expression from the *tetO-Kir2.1.ires.LacZ* transgenic line²⁰ and administered it at different developmental time points (Supplementary Fig. 6a). We were able to monitor the expression of the Kir2.1 transgene by assessing beta-gal activity (Fig. 3b). To determine whether Kir2.1 expression had any effects on early interneuron differentiation, we treated *Dlx5/6-Tta* and *Dlx5/6-eGFP* e15.5-electroporated pregnant mice with Dox at e16.5. Since it takes approximately three days for Dox administration to fully and irreversibly suppress the expression of Kir2.1 and LacZ (Supplementary Fig. 7), in these experiments Kir2.1 expression is shut off from P0 onwards. We found that Kir2.1 expression before P0 had no effect on the laminar position, immunochemical profile, morphology or intrinsic physiological properties of CGE-derived interneurons analyzed at P8-P9 (Fig. 3a, data not shown). Thus, interneuron specification and maturation proceed normally if Kir2.1 is shut off by P0.

In contrast, migration defects persisted when Kir2.1 expression was shut off at P3 (Fig. 3a). Remarkably, despite their abnormal laminar position under these conditions, the morphology of Cr⁺ and Re⁺ subtypes was unperturbed (Fig. 3c-d). The total length and complexity of Cr⁺ and Re⁺ interneuron axonal arbors was not significantly different in Dox-treated *tetO-Kir2.1.ires.LacZ* mice compared to *wild type* controls (Fig. 3d and Supplemental Fig. 6b, d). Similarly, the complexity of the dendritic trees in Kir2.1-expressing Re⁺ interneurons after Dox treatment was similar to that observed in controls (Fig. 3d and Supplemental Fig. 6c). In contrast, both morphological and migratory defects persisted in *tetO-Kir2.1.ires.LacZ* mice in which Kir2.1 expression was turned off from P5 onwards (Supplementary Fig. 8, data not shown). Together these findings revealed that neuronal activity is independently required between P0 and P3 to regulate laminar position and after P3 to control the morphological development of specific interneuron subtypes.

What kinds of activity might be responsible for controlling these distinct aspects of subtype-specific integration at different developmental stages? Experimental evidence suggests that a large proportion of developing neurons in the central nervous system show correlated

spontaneous activity²¹⁻²³. This activity results in prominent cortical activity patterns apparent during the first postnatal week such as glutamate-dependent cortical early network oscillations (cENOs)¹⁶. Interestingly, cortical interneurons have the ability to participate in such activity since they express glutamate receptors at early stages of development²⁴. To explore the possibility that interneuron maturation is regulated by glutamate-driven ionotropic receptor activity, we utilized kynurenic acid, an NMDA and AMPA/Kainate receptor blocker²⁵. We applied either kynurenic acid diluted in PBS (Kyn) or PBS alone (control) subdurally to the brains of *Dlx5/6-eGFP* electroporated mice at P0, P1, P2 and P3 and analyzed interneuron migration and morphology at P8-P9 (Supplementary Fig. 9a and Fig. 4). Migration of all subtypes was normal after Kyn injections at all ages tested (see Supplementary Information). In contrast, we observed morphological defects in Cr⁺ and Re⁺ subtypes in mice injected with Kyn at P3 (but not after administration at earlier ages, i.e. P0, P1, P2). These subtype specific defects were reminiscent of those found in the Kir2.1 experiments (Fig. 4). Specifically, the total axonal length and complexity of Cr⁺ and Re⁺ interneurons was significantly reduced after Kyn treatment (Fig. 4b and Supplementary Fig. 9d, f). Dendritic trees of Re⁺ interneurons in Kyn-treated mice also showed a trend towards a reduction in overall length and a simplified morphology compared to controls (Fig. 4c, Supplementary Fig 9g). In contrast, VIP⁺ interneurons were not affected by Kyn treatment (Fig. 4 and Supplementary Fig. 9b-c). These results indicate that ionotropic glutamate receptor-mediated activity is required after P3 to regulate the subtype specific development of neuronal morphology but does not control their selection of cortical laminae.

To explore the molecular mechanism underlying the activity-dependent maturation of CGE-derived interneuron subtypes, we examined transcriptional programs that operate in these interneurons at early developmental stages²⁶⁻²⁷. Previous experimental evidence indicates that *Dlx1* is essential for both proper cortical migration and morphological development of GABAergic interneurons^{15,26,28}. To determine whether *Dlx1* expression is modulated by activity, we analyzed the expression of DLX protein in control and Kir2.1-electroporated interneurons. We found that Kir2.1-expressing interneurons exhibit lower levels of DLX expression compared to controls at P5 (Fig. 5a, c). Reduced levels of DLX expression are likely to represent attenuated *Dlx1* and/or *Dlx2* expression (see Methods). To confirm that the *Dlx1* transcriptional program is downregulated in Kir2.1-expressing interneurons, we assessed the expression of the neuronal PAS domain protein 1 (NPAS1), a previously described *Dlx1* target. Consistent with a downregulation of *Dlx1*, we found that the levels of NPAS1 in Re⁺ subtypes were reduced upon Kir2.1 expression (Supplementary Fig. 10).

Another gene that was also shown to be a target of *Dlx* genes is ELMO1, an evolutionarily conserved Rac-activator protein¹⁴⁻¹⁵. Since ELMO1 has been implicated in cytoskeletal reorganization and migration in the immune system^{14,29} and is significantly downregulated in *Dlx1/2* knockout mice¹⁵, which exhibit severe interneuron migration defects, we assessed its expression in developing GABAergic interneurons (Fig. 5b). We found that ELMO1 is expressed by Re⁺ and Cr⁺, but not VIP⁺ subtypes and is downregulated upon Kir2.1 expression (Fig. 5b-c). To investigate whether loss of ELMO1 function can lead to defects in interneuron migration and morphological maturation, we co-electroporated e15.5 CGE-derived interneurons with a dominant negative form of the ELMO1 protein that impairs Rac

activation, *Dlx5/6-Elmo1_TN558.FLAG*³⁰, and *Dlx5/6-eGFP*. At P9, we detected immunoreactivity against the FLAG epitope indicating that there is proper expression of the dominant negative protein in electroporated interneurons (Fig. 5d, inset). Interestingly, whereas electroporated Re⁺ and Cr⁺ interneurons show normal morphological development, these interneurons were found to be distributed to deeper layers compared to those of *Dlx5/6-eGFP* controls (Fig. 5d, f; data not shown). In agreement with the lack of ELMO1 expression in VIP⁺ interneurons, neither their migration nor their morphology was affected by overexpression of the dominant negative protein (data not shown). Our observations suggest that ELMO1 is necessary for the proper radial migration of Re⁺ and Cr⁺ subtypes. To address whether the reduction in ELMO1 expression is responsible for the abnormalities in laminar migration observed in Kir2.1-expressing Re⁺ interneurons, we co-electroporated e15.5 interneurons with a *Dlx5/6-Elmo1* construct together with *Dlx5/6-Kir2.1* and *Dlx5/6-eGFP* plasmids. We reasoned that the recovery of ELMO1 expression in Re⁺ and Cr⁺ Kir2.1-electroporated interneurons would rescue their migratory defects. Remarkably, the migration but not the morphology of these subtypes appear normal in Kir2.1-electroporated interneurons that co-expressed ELMO1 at P9 (Fig. 5e-f, data not shown). As expected, neither migratory nor morphological defects were detected in VIP⁺ interneurons. In contrast, expression of *Dlx5/6-Elmo1* plasmid in the absence of *Dlx5/6-Kir2.1* did not affect migration or morphological maturation of Re⁺, Cr⁺ and VIP⁺ subtypes (data not shown). These results suggest that ELMO1 is necessary and sufficient for the proper activity-dependent migration of Re⁺ interneurons. Taken together, our results indicate that the molecular machinery directing the maturation of Re⁺, Cr⁺ interneurons, including *Dlx1*, *Npas1* and *Elmo1*, has evolved to be controlled by activity during development.

A role for *Dlx* genes in both interneuron migration and morphological development has been previously reported¹⁵; however, a link between *Dlx* expression and neuronal activity has not been established. Our studies suggest that *Dlx1* expression and associated downstream targets are selectively regulated by activity in at least some interneuron subtypes. Specifically, *Dlx* genes induce the expression of *Elmo1*¹⁵ which is required for proper laminar migration of Re⁺ and Cr⁺ subtypes. Although we currently provide only correlative evidence for the link between activity-regulated expression of *Dlx1* and morphological development, the alteration in interneuron morphology observed in *Dlx1* null mutants supports this contention²⁸. These findings suggest that genetic programs initiated at the progenitor stage are modulated during development by activity. Thus, our studies indicate that the role of early network activity in shaping the development of specific neuronal subtypes in the central nervous system is greater than is presently appreciated.

Method summary

Mouse strains and *in utero* electroporation

Pregnant wild type and genetically modified mice (see Methods) were electroporated at 15 days of gestation (e15.5) using a standard *in utero* electroporation technique³². The plasmids used in the electroporation experiments were generated using standard cloning techniques.

***In situ* hybridization and immunohistochemistry**

In situ hybridization and immunohistochemistry were performed as previously described³³. For morphological reconstruction, vibratome sections were fixed and incubated overnight at 4 C with selected antibodies.

Quantification of interneuron layer distribution

The proportion of Cr⁺, Re⁺ and VIP⁺ interneurons over the total number of electroporated interneurons across cortical layers was calculated in all cryostat tissue sections from individual brains. Tbr1 immunolabeling was used to delineate cortical layers II/III and V at P5-P8.

Kynurenic acid treatment

Dlx5/6-eGFP electroporated pups were anesthetized by hypothermia. Kynurenic acid (300 nM, Sigma-Aldrich, USA) diluted in PBS or pure PBS (controls) were injected at P0, P2 and P3. Treated brains in which electroporated interneurons were found in the vicinity of the injection site were used for analysis to minimize variability due to drug diffusion.

Electrophysiology

Whole-cell patch-clamp electrophysiological recordings were performed on eGFP-expressing cells in acute brain slices prepared from P2-P18 animals. Whole-cell recordings were made from randomly selected eGFP-positive neurons located in upper layers (I-III) of the somatosensory cortex. Experiments were performed in both current-clamp and voltage-clamp modes.

Neuronal morphology analysis

Images of interneurons were obtained with a confocal microscope, analyzed with LSM Image Browser, and reconstructed with Neurolucida software (Version 9). To assess the length and complexity of dendritic and axonal arborizations, we quantified the number of nodes (points from which two or more branches arose) and ends (terminal branches) in each of these trees with Neurolucida Explorer.

Statistical analysis

Statistical analysis was performed by using Student's test (two-tailed distribution, homoscedastic) unless otherwise stated.

Detailed methods on the mouse strains, animal surgery and electrophysiology protocols can be found in Methods.

Materials and Methods

Mouse strains

Pregnant Swiss Webster mice (Taconic) were electroporated at 15 days of gestation (e15.5). The *tetO-Kir2.1.ires.LacZ* transgenic mouse line was provided by Joseph Gogos²⁰. Doxycycline was administered in mouse feed (20 g/kg of feed) at selected time points

(e16.5, P0, P3). The *Gad67-GFP* (gift of Yuchio Yanagawa) mouse line³¹ was available in the Fishell lab. Details on the genotyping of the mouse strains have been described elsewhere¹².

***In utero* electroporation**

Pregnant mice were electroporated using a standard *in utero* electroporation technique³². In brief, a timed pregnant mouse was anaesthetized and embryos were injected through the uterine wall in one lateral ventricle with 1-2 μ l of DNA (3 μ g/ μ l). Fast green was used for visualization of the DNA solution. DNA was delivered by a glass needle operated with a mouse pipette. Five square 50 ms pulses at 40 mV with a 950 ms interval long were delivered with a 5 mm paddle electrode (CUY650P5, Bex Co., LTD) using an electroporator (CUY21, Bex Co., LTD). After electroporation, the uterus was placed back in the abdominal cavity and the mouse was sutured. The mice were kept on a warm plate (Fine Science Tools) through surgery to minimize hypothermia. After surgery, mice recovered in a humidified chamber at 30 C for 2-3 hours. Mouse colony maintenance and handling was performed in compliance with the protocols approved by the Institutional Animal Care and Use Committee of the New York University School of Medicine.

The plasmids used in the electroporation experiments were generated using standard cloning techniques. The mouse *Kir2.1*, tetracycline transactivator (*Tta*), *mCherry*, *eGFP*, *Elmo1* and *Elmo1.TN558.FLAG* cDNAs were each individually cloned into a *Dlx5/6-Pmin-polyA* plasmid. Since GFP expression was not detected in brains electroporated with a *Dlx-5/6-Kir2.1.ires.eGFP* polycistronic plasmid, the *Dlx5/6-eGFP* plasmid was co-electroporated with *Dlx5/6-Kir2.1*, *Dlx5/6-Tta*, *Dlx5/6-Elmo1* or *Dlx5/6-Elmo1.TN558.FLAG* plasmids at equivalent molar concentrations to ensure high levels of co-expression. The detection of similar levels of GFP expression in *Dlx5/6-eGFP* and *Dlx5/6-eGFP/Dlx5/6-Kir2.1* electroporated interneurons indicates that transcription driven by this enhancer is not affected by *Kir2.1* expression. For generation of CAG-mCherry, the mCherry cDNA was cloned into a CAG-MCS vector. Expression of the *tetO-Kir2.1.ires.LacZ* upon electroporation with the *Dlx5/6-Tta* plasmid was detected by processing tissue sections for beta-gal staining²⁰.

***In situ* hybridization and immunohistochemistry**

In situ hybridization was performed as described³³ using a full length *Kir2.1* dig-labeled probe. Immunohistochemistry on 20 μ m tissue cryostat sections was previously described³⁴. For morphological reconstruction, 250 μ m thick vibrotome sections were fixed for 2 hours and incubated overnight (ON) at 4 C with selected antibodies. Sections were washed in PBS for several hours and incubated at 4 C ON with donkey secondary antibodies (Jackson labs). Primary antibodies used in the experiments include rat anti-GFP (1:2000; Nacalai Tesque), mouse anti-Reelin (CR50) (1:500; MBL), rabbit anti-VIP (1:1000, Immunostar), mouse anti-calretinin (1:1500; Millipore Bioscience Research Reagents), rabbit anti-Tbr1 (1:1000 Abcam), goat anti-Tbr1 (1:1000 Abcam), rabbit anti-Pan-DLX (a gift from Jhumku Kohtz), rabbit anti-NPAS1 (a gift from Miura Masayuki), goat anti-ELMO1 (1:250 Millipore) and mouse anti-FLAG (1:200 Sigma Aldrich).

Quantification of cell death

Caspase 3 activity (Clontech) was assessed on cryostat sections of P8 brains electroporated with *Dlx5/6-eGFP* or *Dlx5/6-eGFP* and *Dlx5/6-Kir2.1* plasmids. The percentage of Caspase3 immunoreactive interneurons that co-express GFP over the total number of GFP-expressing interneurons was counted on five Kir2.1-electroporated mice and five control mice.

Quantification of interneuron layer distribution

The proportion of Cr⁺, Re⁺ and VIP⁺ interneurons over the total number of electroporated interneurons across cortical layers was calculated in all cryostat tissue sections from individual brains. Analysis was performed on four *wild type* (74 interneurons) and six *tetO-Kir2.1.ires.LacZ* (150 interneurons) mice co-electroporated with *Dlx5/6-Tta* and *Dlx5/6-eGFP* plasmids.

Kynurenic acid treatment

Dlx5/6-eGFP electroporated pups were anesthetized by hypothermia on ice for two minutes. The pups were protected with cloth to prevent frostbite. Kynurenic acid²⁵ (300 nM, Sigma-Aldrich, USA) diluted in PBS and pure PBS (controls) was injected at P0, P2 and P3. Fast green was used for visualization. A small window was opened in the skull with needles and solution was injected in the subdural space on the electroporated side. The skull opening was closed with cyanoacrylate adhesive. Pups were allowed to recover in a humidified chamber at 34 C for 5-10 minutes and another 20 minutes at room temperature before putting them back in their cages. Treated brains in which electroporated interneurons were found in the vicinity of the injection site were used for analysis to minimize variability due to drug diffusion. Kynurenic (Kyn) injections at P0, P1, P2 and P3 had no effect on interneuron migration. Therefore, we averaged the values obtained for laminar distribution in six control (110 interneurons) and six Kyn-treated (165 interneurons) mice electroporated with a *Dlx5/6-eGFP* plasmid. Analysis was performed at P8-P9.

Electrophysiology

Whole-cell patch-clamp electrophysiological recordings were performed on eGFP-expressing cells in acute brain slices prepared from P8-P18 animals. Briefly, animals were decapitated and the brain was dissected out and transferred to physiological Ringer's solution (ACSF) cooled down to 4°C of the following composition (mM): 125 NaCl, 2.5 KCl, 25 NaHCO₃, 1.25 NaH₂PO₄, 1 MgCl₂, 2 CaCl₂ and 20 glucose. The brain was then glued to a stage and 250 µm-thick slices were cut using a vibratome (Vibratome 3000 EP). The slices were allowed to recover in recording ACSF at room temperature for at least 45 min. before recording. Acute slices were then placed in a recording chamber mounted on the stage of an upright microscope (Axioscope, Zeiss, Germany) equipped with immersion differential interference contrast objectives (5x, 40x) coupled to an infrared camera system (Zeiss), superfused at a rate of 1-2 ml/min. with oxygenated recording ACSF and maintained at a temperature of 31°C. An eGFP filter was used to visualize the fluorescent interneurons in epifluorescence.

Whole-cell recordings were made from randomly selected eGFP-positive neurons located in upper layers (I-III) of the somatosensory cortex. Patch electrodes were made from borosilicate glass (Harvard Apparatus), had a resistance of 4–8 M and were filled with a solution containing (in mM): 128 K-gluconate, 4 NaCl, 0.3 Na-GTP, 5 Mg-ATP, 0.0001 CaCl₂, 10 HEPES, 1 glucose, and 5 mg/ml biocytin (Sigma). Experiments were performed in current-clamp mode using the Axoclamp 2B (Molecular Devices) or the Axopatch 200B amplifier and in voltage clamp using the latter.

Access resistance was always monitored to ensure the stability of recording conditions. Cells were only accepted for analysis if the initial series resistance was less than or equal to 40 M Ω and did not change by more than 20% throughout the recording period. The series resistance was compensated online by at least ~ 50% in voltage-clamp mode to reduce voltage errors. No correction was made for the junction potential between the pipette and the ACSF.

For Kir2.1 conductance assessment a series of voltage steps in 10-mV increments were applied every 1-5 s in voltage clamp from -140mV to 0mV starting from -70mV after a prepulse down to -90mV so as to deactivate any Kir2.1 channels that had entered inactivated states.

Firing and passive membrane properties were recorded in current clamp mode by applying a series of sub- and supra-threshold current steps. The resting membrane potential (V_{rest}) was ascertained in current clamp right after rupturing the patch by applying zero current.

All drugs were applied to the recording preparation through the bath. Salts used in the preparation of the intracellular recording solution and ACSF were obtained from Sigma-Aldrich, USA. Kynurenic acid, bicuculline and DNQX were also purchased from Sigma-Aldrich, USA.

Neuronal morphology analysis

Images of interneurons were obtained with a Zeiss (LSM 510 Meta) confocal microscope, analyzed with LSM Image Browser, and reconstructed with NeuroLucida software (Version 9). Morphological defects were observed in >50 interneurons (>10 brains) of each subtype (Cr and Re) after Kir2.1 electroporation and Kyn treatment. In addition, analysis of morphology after Dox administration in *tetO-Kir2.1.ires.LacZ* mice co-electroporated with *Dlx5/6-Tta* and *Dlx5/6-eGFP* plasmids was performed in >20 interneurons (>4 brains). Similarly, >70 interneurons (>10 brains) were analyzed in control experiments. A few of these interneurons were chosen for reconstruction. The total length and complexity of axonal arbors and dendritic trees was scored in confocal stacks (optical slice thickness, 4 μ m; stack size 50-100 μ m) including all the neuronal processes. Interneurons are oriented such that the top of the figure panel points towards the pia and the bottom to the lateral ventricle. To assess the length and complexity of dendritic and axonal arborizations, we quantified the number of nodes (points from which two or more branches arose) and ends (terminal branches) in each of these trees with NeuroLucida Explorer. Total length and complexity of neuronal processes were scored in the same set of reconstructed interneurons for each

experiment. GFP labeling in electroporated interneuron was indistinguishable from that of streptavidin fills.

Statistical analysis

Statistical analysis was performed by using Student's test (two-tailed distribution, homoscedastic) unless otherwise stated.

Supplementary Material

Refer to Web version on PubMed Central for supplementary material.

Acknowledgements

We are grateful to Renata Batista-Brito, Eugenia Chiappe, Rosa Cossart, Jeremy Dasen, Julia Kaltschmidt, SooHyun Lee, Jens Hjerling Leffler, Michael Long, David Pisapia and Bernardo Rudy for comments on the manuscript. We thank Lihong Yin for technical assistance. We are indebted to Kodi Ravichandran from providing the ELMO1 constructs. NVD and TK are both supported by grants from The Patterson Trust. Research in the Fishell laboratory is supported by National Institutes of Health – National Institute of Mental Health–National Institute of Neurological Disorders and Stroke Grants and support from the Simons Foundation.

References

- Blankenship AG, Feller MB. Mechanisms underlying spontaneous patterned activity in developing neural circuits. *Nat Rev Neurosci.* 2010; 11:18–29. [PubMed: 19953103]
- Wong RO, Chernjavsky A, Smith SJ, Shatz CJ. Early functional neural networks in the developing retina. *Nature.* 1995; 374:716–718. [PubMed: 7715725]
- Penn AA, Riquelme PA, Feller MB, Shatz CJ. Competition in retinogeniculate patterning driven by spontaneous activity. *Science.* 1998; 279:2108–2112. [PubMed: 9516112]
- Huberman AD, et al. Architecture and activity-mediated refinement of axonal projections from a mosaic of genetically identified retinal ganglion cells. *Neuron.* 2008; 59:425–438. [PubMed: 18701068]
- Spitzer NC. Electrical activity in early neuronal development. *Nature.* 2006; 444:707–712. [PubMed: 17151658]
- Root CM, Velazquez-Ulloa NA, Monsalve GC, Minakova E, Spitzer NC. Embryonically expressed GABA and glutamate drive electrical activity regulating neurotransmitter specification. *J Neurosci.* 2008; 28:4777–4784. [PubMed: 18448654]
- Cancedda L, Fiumelli H, Chen K, Poo MM. Excitatory GABA action is essential for morphological maturation of cortical neurons in vivo. *J Neurosci.* 2007; 27:5224–5235. [PubMed: 17494709]
- Wang CL, et al. Activity-dependent development of callosal projections in the somatosensory cortex. *J Neurosci.* 2007; 27:11334–11342. [PubMed: 17942728]
- McBain CJ, Fisahn A. Interneurons unbound. *Nat Rev Neurosci.* 2001; 2:11–23. [PubMed: 11253355]
- Ascoli GA, et al. Petilla terminology: nomenclature of features of GABAergic interneurons of the cerebral cortex. *Nat Rev Neurosci.* 2008; 9:557–568. [PubMed: 18568015]
- Batista-Brito R, Fishell G. The developmental integration of cortical interneurons into a functional network. *Curr Top Dev Biol.* 2009; 87:81–118. [PubMed: 19427517]
- Miyoshi G, et al. Genetic fate mapping reveals that the caudal ganglionic eminence produces a large and diverse population of superficial cortical interneurons. *J Neurosci.* 2010; 30:1582–1594. [PubMed: 20130169]
- Karube F, Kubota Y, Kawaguchi Y. Axon branching and synaptic bouton phenotypes in GABAergic nonpyramidal cell subtypes. *J Neurosci.* 2004; 24:2853–2865. [PubMed: 15044524]
- Gumienny TL, et al. CED-12/ELMO, a novel member of the CrkII/Dock180/Rac pathway, is required for phagocytosis and cell migration. *Cell.* 2001; 107:27–41. [PubMed: 11595183]

15. Cobos I, Borello U, Rubenstein JL. Dlx transcription factors promote migration through repression of axon and dendrite growth. *Neuron*. 2007; 54:873–888. [PubMed: 17582329]
16. Allene C, Cossart R. Early NMDA receptor-driven waves of activity in the developing neocortex: physiological or pathological network oscillations? *J Physiol*. 2010; 588:83–91. [PubMed: 19917570]
17. Garaschuk O, Linn J, Eilers J, Konnerth A. Large-scale oscillatory calcium waves in the immature cortex. *Nat Neurosci*. 2000; 3:452–459. [PubMed: 10769384]
18. Dupont E, Hanganu IL, Kilb W, Hirsch S, Luhmann HJ. Rapid developmental switch in the mechanisms driving early cortical columnar networks. *Nature*. 2006; 439:79–83. [PubMed: 16327778]
19. Stenman J, Toresson H, Campbell K. Identification of two distinct progenitor populations in the lateral ganglionic eminence: implications for striatal and olfactory bulb neurogenesis. *J Neurosci*. 2003; 23:167–174. [PubMed: 12514213]
20. Yu CR, et al. Spontaneous neural activity is required for the establishment and maintenance of the olfactory sensory map. *Neuron*. 2004; 42:553–566. [PubMed: 15157418]
21. Yang JW, Hanganu-Opatz IL, Sun JJ, Luhmann HJ. Three patterns of oscillatory activity differentially synchronize developing neocortical networks in vivo. *J Neurosci*. 2009; 29:9011–9025. [PubMed: 19605639]
22. Khazipov R, Luhmann HJ. Early patterns of electrical activity in the developing cerebral cortex of humans and rodents. *Trends Neurosci*. 2006; 29:414–418. [PubMed: 16713634]
23. McCabe AK, Chisholm SL, Picken-Bahrey HL, Moody WJ. The self-regulating nature of spontaneous synchronized activity in developing mouse cortical neurones. *J Physiol*. 2006; 577:155–167. [PubMed: 16945966]
24. Manent JB, Jorquera I, Ben-Ari Y, Aniksztejn L, Represa A. Glutamate acting on AMPA but not NMDA receptors modulates the migration of hippocampal interneurons. *J Neurosci*. 2006; 26:5901–5909. [PubMed: 16738232]
25. Stone TW. Neuropharmacology of quinolinic and kynurenic acids. *Pharmacol Rev*. 1993; 45:309–379. [PubMed: 8248282]
26. Anderson SA, Eisenstat DD, Shi L, Rubenstein JL. Interneuron migration from basal forebrain to neocortex: dependence on Dlx genes. *Science*. 1997; 278:474–476. [PubMed: 9334308]
27. Wonders CP, Anderson SA. The origin and specification of cortical interneurons. *Nat Rev Neurosci*. 2006; 7:687–696. [PubMed: 16883309]
28. Cobos I, et al. Mice lacking Dlx1 show subtype-specific loss of interneurons, reduced inhibition and epilepsy. *Nat Neurosci*. 2005; 8:1059–1068. [PubMed: 16007083]
29. Ravichandran KS, Lorenz U. Engulfment of apoptotic cells: signals for a good meal. *Nat Rev Immunol*. 2007; 7:964–974. [PubMed: 18037898]
30. Park D, et al. BAI1 is an engulfment receptor for apoptotic cells upstream of the ELMO/Dock180/Rac module. *Nature*. 2007; 450:430–434. [PubMed: 17960134]
31. Tamamaki N, et al. Green fluorescent protein expression and colocalization with calretinin, parvalbumin, and somatostatin in the GAD67-GFP knock-in mouse. *J Comp Neurol*. 2003; 467:60–79. [PubMed: 14574680]
32. Saito T. In vivo electroporation in the embryonic mouse central nervous system. *Nat Protoc*. 2006; 1:1552–1558. [PubMed: 17406448]
33. Butt SJ, et al. The requirement of Nkx2-1 in the temporal specification of cortical interneuron subtypes. *Neuron*. 2008; 59:722–732. [PubMed: 18786356]
34. Miyoshi G, Butt SJ, Takebayashi H, Fishell G. Physiologically distinct temporal cohorts of cortical interneurons arise from telencephalic Olig2-expressing precursors. *J Neurosci*. 2007; 27:7786–7798. [PubMed: 17634372]

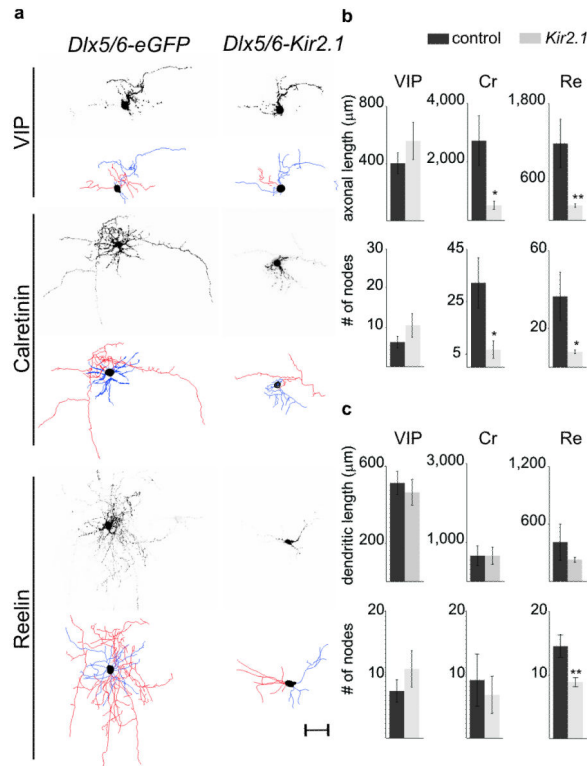


Figure 1. Defective morphology of Cr⁺ and Re⁺ interneuron subtypes resulting from Kir2.1 expression

a. Representative examples of P8 VIP⁺, Cr⁺ and Re⁺ interneurons in mice electroporated at e15.5 with *Dlx5/6-eGFP* (control) or *Dlx5/6-eGFP, Dlx5/6-Kir2.1* plasmids at e15.5. Photomicrographs of eGFP expression and corresponding neuroLucida reconstructions depicting axons (red), dendrites (blue) and somata (black). Scale bar: 50 μm . Morphometric analysis of control and Kir2.1-expressing VIP⁺, Cr⁺ and Re⁺ subtypes including the total length of axonal arbors (top) and number of axonal nodes (bottom). c. total length of dendritic trees (top) and number of dendritic nodes (bottom) in the same subtypes. Mean values (\pm SEM) were obtained from >4 reconstructed interneurons each in *Dlx5/6-eGFP* and *Dlx5/6-eGFP, Dlx5/6-Kir2.1* electroporated mice. Paired t-test: *, P<0.05; **, P<0.01

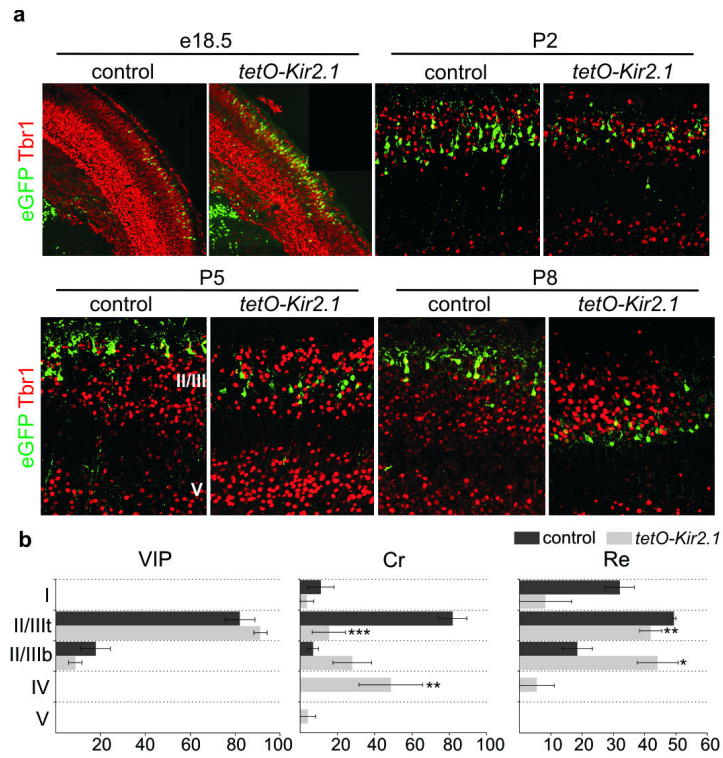


Figure 2. Neuronal activity is essential for the proper laminar migration of selective interneuron subtypes

a. Laminar positioning of electroporated interneurons in *wild type* mice (control) and *tetO-Kir2.1.ires.LacZ* littermates both co-electroporated with *Dlx5/6-Tta* and *Dlx5/6-eGFP* plasmids at e15.5. Tbr1 expression delineates layers II/III and V at P5-P8. Representative examples taken from the analysis of 4 control and 6 *tetO-Kir2.1.ires.LacZ* electroporated mice for each developmental stage. b. Quantification of the distribution of VIP⁺, Cr⁺ and Re⁺ interneuron subtypes across cortical layers at P8. Due to the lack of selective molecular markers to distinguish between cortical layer II and III at P8-P9, we divided these layers collectively into II/III_{top} (II/III_t) and II/III_{bottom} (II/III_b). Mean percentage values (\pm SEM) were obtained from 4 *wild type* and 6 *tetO-Kir2.1.ires.LacZ* electroporated mice. Paired t-test: *, P<0.05; **, P<0.01; ***, P<0.001.

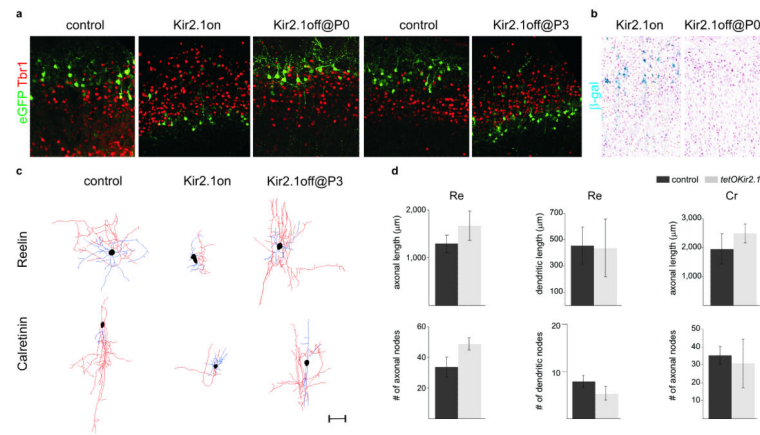


Figure 3. Specific interneuron subtypes require activity for migration and morphological maturation at two distinct stages of development

a. Laminar positioning of P8 electroporated interneurons in *wild type* mice (control) and *tetO-Kir2.1.ires.LacZ* mice both co-electroporated with *Dlx5/6-Tta* and *Dlx5/6-eGFP* plasmids at e15.5. Mice received either no treatment (Kir2.1on); or were treated with Dox at e16.5 (Kir2.1off @ P0 onwards); or with Dox at P0 (Kir2.1off @ P3 onwards). b. β-galactosidase activity in P8 *tetO-Kir2.1.ires.LacZ* mice co-electroporated with *Dlx5/6-Tta* and *Dlx5/6-eGFP* plasmids either untreated or treated with Dox at e16.5 (Kir2.1off @ P0 onwards). c. Neurolucida reconstructions of Cr⁺ and Re⁺ interneurons in *wild type* (control) and *tetO-Kir2.1.ires.LacZ* mice both co-electroporated with *Dlx5/6-Tta* and *Dlx5/6-eGFP* plasmids. Mice received either no Dox treatment (Kir2.1on) or Dox at P0 (Kir2.1off @ P3 onwards). Axons are shown in red, dendrites in blue and somata in black. Scale bar: 50 μm d. Quantification of dendritic and axonal morphology in control and experimental Cr⁺ and Re⁺ interneurons in *tetO-Kir2.1.ires.LacZ* mice after Dox administration at P0. Mean percentage values (±SEM) were obtained from >3 reconstructed interneurons each in Dox-treated *wild type* and *tetO-Kir2.1.ires.LacZ* mice for each subtype analyzed at P8.

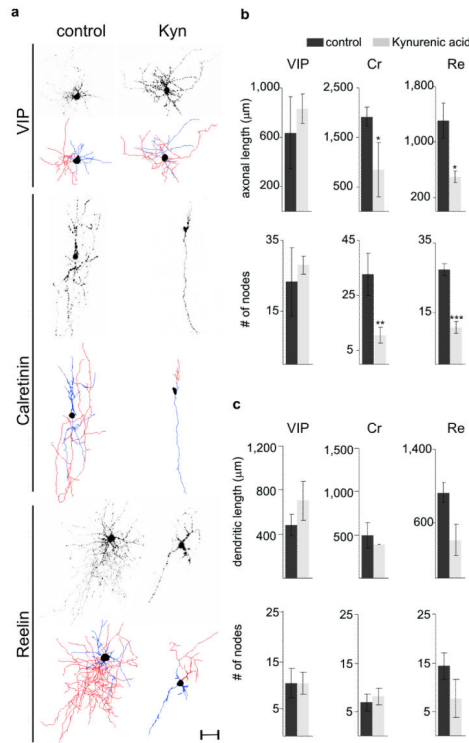


Figure 4. Ionotropic glutamate receptor blockade mimics the effects of Kir2.1 expression on Cr⁺ and Re⁺ interneuron morphology

a. Representative examples of P8 VIP⁺, Cr⁺ and Re⁺ interneurons in *Dlx5/6-eGFP* electroporated mice at e15.5 injected with PBS (control) or kynurenic acid (Kyn) at P3 and corresponding neuroLucida reconstructions depicting axons (red), dendrites (blue) and somata (black). Scale bar: 50 μm b-c. Morphometric analysis of control and kynurenic-treated neurons including the total length of axonal arbors (b, top) and the number of axonal nodes (b, bottom), and the total length of dendritic trees (c, top) and number of dendritic nodes (c, bottom) in VIP⁺, Cr⁺ and Re⁺ subtypes. Mean percentage values (±SEM) were obtained from 3 electroporated interneurons each in control and Kyn-treated mice for each subtype. Paired t-test: *, P<0.05; **, P=0.05; ***, P<0.01

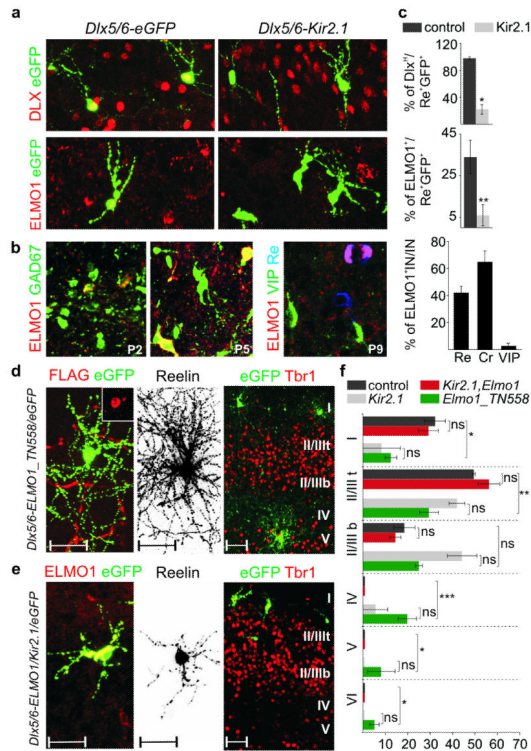


Figure 5. Activity-dependent expression of ELMO1 regulates CGE-derived interneuron migration

- a. Expression of *Dlx* genes and ELMO1 at P5 in *Dlx5/6-eGFP* and *Dlx5/6-Kir2.1* electroporated interneurons at e15.5.
- b. Expression of ELMO1 in *GAD67-GFP* transgenic mice at P2 and P5. Selective expression of ELMO1 in CGE-derived interneuron subtypes at P9. Quantification of ELMO1 expression in Re^+ , Cr^+ and VIP^+ interneurons (IN) at P9 (right). Mean percentage values (\pm SEM) were obtained from >70 interneurons for each subtype.
- c. Quantification of DLX^H and ELMO1 expression in *Dlx5/6-eGFP* (control) and *Dlx5/6-Kir2.1* Re^+ e15.5-electroporated interneurons at P5. Mean percentage values (\pm SEM) were obtained from >20 interneurons each in control and *Kir2.1* electroporated mice for each quantification.
- d. Electroporation of *Dlx5/6-Elmo1_TN558.FLAG* plasmid at e15.5. FLAG immunoreactivity is detected in electroporated interneurons at P9 (inset). Neuronal morphology of a Re^+ interneuron and laminar distribution of electroporated interneurons at P9. Representative examples from 4 electroporated mice.
- e. Co-electroporation of *Dlx5/6-Elmo1* and *Dlx5/6-Kir2.1* plasmids at e15.5. ELMO1 expression in electroporated interneurons at P9. Morphological defects of an electroporated Re^+ interneuron and laminar distribution of electroporated interneurons. Representative examples from 6 electroporated mice.
- f. Quantification of the distribution of Re^+ interneurons across cortical layers at P9 upon expression of different plasmids. Mean percentage values (\pm SEM) were obtained from >80 interneurons for each group. Values for control and *Dlx5/6-Kir2.1* alone groups are repeated from Figure 2 to facilitate comparison between groups. The large bracket indicates

comparison between the control and *Dlx5/6-Elmo1_TN558.FLAG* electroporated interneurons.

Paired t-test: *, $P < 0.05$; **, $P < 0.01$; ***, $P < 0.0001$. DLX^H, high level of DLX protein expression. Scale bars for d and e: 50 μm

Author Manuscript

Author Manuscript

Author Manuscript

Author Manuscript